J. Fluid Mech. (1999), *vol.* 388, *pp.* 335–354. Printed in the United Kingdom

Scattering and near-trapping of water waves by axisymmetric topography

By P. G. CHAMBERLAIN AND D. PORTER

Department of Mathematics, The University of Reading, PO Box 220, Whiteknights, Reading, RG6 6AX, UK

(Received 11 June 1998 and in revised form 21 December 1998)

The scattering of plane surface water waves by both surface-piercing and submerged axisymmetric bed formations has been investigated by a number of authors. We extend previous contributions in two ways: we employ the recently derived modified mild-slope equation to approximate the fluid motion and we consider arbitrary axisymmetric topography, subject only to the restriction imposed by the mild-slope approximation. We thereby derive a robust method for calculating the scattered wave field for the small seabed slopes typical of most real situations and make a contribution to the phenomena of near-resonance and near-trapping over submerged axisymmetric shoals, which have previously been detected for only one idealized bedform.

1. Introduction

The problem of the linear scattering of a plane monochromatic water wave by axisymmetric depth perturbations on an otherwise horizontal bed has been used for some time to simulate ocean wave motions around circular islands and over shoals. Homma (1950) examined a particular example of surface-piercing topography consisting of a vertical circular cylinder surmounting a submerged shoal in the form of a paraboloid. By restricting attention to the special case in which the apex of the paraboloid lies at the level of the undisturbed free surface, an analytic solution of the corresponding linearized shallow water equations is possible. On this basis, Homma showed that unexpectedly large-amplitude waves are possible over the shoal at certain incident wave frequencies. Vastano & Reid (1967) subsequently produced accurate numerical results for Homma's problem, by using a finite difference scheme on a truncated domain.

Experimental evidence of wave energy trapping over shoaling topography, such as that produced by Snodgrass, Munk & Miller (1962), stimulated further work and, in particular, led to a significant theoretical contribution by Longuet-Higgins (1967), who considered wave motions in the presence of a submerged circular cylinder, again using shallow water theory. As in the case examined by Homma (1950), an analytic solution is possible, but it can only be interpreted by using numerical calculations or asymptotic approximations. Longuet-Higgins found that trapped waves are not possible over a submerged circular sill since there is inevitably a leakage of energy to infinity. Nevertheless, at certain frequencies, 'nearly trapped' waves can exist in the sense that this energy leakage is extremely small. Expressed in other terms, near-trapping arises when the underlying homogeneous problem has a non-trivial solution at a complex value of the frequency which has a very small imaginary part. In

relation to the forced problem of plane wave scattering, near-trapping corresponds a large response over the topography which may be described as 'near-resonance'. The real part of the complex near-trapping frequency and the frequency at which near-resonance occurs do not normally coincide but can be extremely close. In other contexts, complex resonant frequencies are known as scattering frequencies. This is the terminology used by Hazard & Lenoir (1993), for example, in their examination of a three-dimensional elastic body floating on water of uniform finite depth.

Summerfield (1972) confirmed Longuet-Higgins' (1967) results and extended them to the problem in which a second, surface-piercing, circular cylinder is mounted on the submerged circular sill, so as to model an island surrounded by an underwater shelf. Shallow water theory was again used by Summerfield, but experimental evidence suggested that it tended to over-estimate near-resonant responses. Black, Mei & Bray (1971) had already considered the scattering problem for the submerged circular sill on the basis of full linear theory, but they did not encounter near-resonance. Renardy (1983) therefore addressed the same problem specifically to examine this phenomenon and concluded that shallow water theory does indeed exaggerate free-surface amplitudes in the context of near-resonance. This outcome prompted Miles (1986) to examine the full linear solution in the 'narrow aperture' limit, in which the fraction over the overall fluid depth above the sill tends to zero, where the strongest near-resonance occurs. Miles confirmed Longuet-Higgins' (1967) results in the long wave limit, and identified an error in Renardy's deductions.

An alternative approximation to full linear theory, the mild-slope equation, had been developed by Lozano & Meyer (1976), in order to conduct an analytic investigation of the trapping of waves around circular islands with a small off-shore seabed slopes. For this realistic model, Lozano & Meyer proved the existence of eigenmodes with small imaginary parts and therefore of nearly trapped waves. Smith & Sprinks (1975) gave an independent derivation of the mild-slope equation at more or less the same time and developed a numerical solution method for conical islands, based on a modal decomposition and an integral equation technique. The computed results for three such islands compare well with those obtained earlier by Lautenbacher (1970) using shallow water theory. However, Smith & Sprinks found that the largest responses occur outside the shallow water régime and that the magnitude of these responses increases with the mode number.

More recently, Zhu & Zhang (1996) have used numerical solutions of the mild-slope equation to examine wave diffraction around a circular island formed by a cylinder mounted on a right cone. As in the case of the geometry considered by Homma (1950), a judicious location of the cone ensures that an analytic solution is possible if shallow water theory is invoked and Zhu & Zhang compare this solution with the corresponding numerical solution of the mild-slope equation. Inevitably, the solutions correspond for long waves, as the mild-slope equation reduces to the shallow water equation in the long wave limit. For shorter waves, shallow water theory generally predicts greater amplitudes at the coastline than the more accurate mild-slope equation. Curiously, Zhu & Zhang present only this comparative study and do not refer to near-resonance or near-trapping.

In addition to the derivations of the mild-slope equation by Lozano & Meyer (1976) and Smith & Sprinks (1975) already mentioned, further derivations were given by Berkhoff (1973, 1976) for the purpose of improving on the shallow water model in general diffraction and refraction problems in coastal engineering problems. More recently, Chamberlain & Porter (1995) developed the modified mild-slope equation which contains additional terms involving the slope and curvature of the bed. One

aspect of this re-appraisal of the mild-slope approximation, described by Porter & Staziker (1995), is that it shows that the apparent accuracy of the original mild-slope equation is only achieved where the bed slope is discontinuous if jump conditions are imposed. This observation improves the applicability of the mild-slope equation, in the sense measured in a particular test problem by Booij (1983), from slopes of 1 in 3 to 1 in 1. Xu & Panchang (1993) have recently devised a finite difference scheme to solve the mild-slope equation and they returned to the work of Homma (1950) to provide an example of axisymmetric scattering.

In the present work, we use the modified mild-slope equation to examine scattering and trapping by axisymmetric topography, with the main emphasis on wholly submerged bedforms. The circular sill remains the only topography in this category which has previously received attention, despite the interesting results obtained by Longuet-Higgins (1967). The modified mild-slope equation subsumes the shallow water equation but is more general in that it can be used across the whole frequency range. Judged by its performance in two-dimensional scattering problems, it provides accurate results as long as the bed slope is not too large.

Although we develop solution techniques which are capable of dealing with scattering and trapping for arbitrary axisymmetric topography, we can only present a limited selection of results. Apart from comparing our calculations with those of Xu & Panchang (1993) to make contact with previous work, we therefore restrict attention for the most part to one particular submerged shoal and examine this in some detail. The results given for the selected topography are typical of many that we have obtained for other topographies.

The overall problem is formulated in § 2; we consider scattering in § 3 and near-resonance and near-trapping together in § 4.

2. Formulation

Let r, θ and z be cylindrical coordinates with z directed vertically upwards and such that $z = 0$ is the undisturbed free surface of a fluid. We suppose that this fluid is incompressible, inviscid and is in irrotational motion, periodic in the time t, above a bed of varying quiescent depth $h = h(r, \theta)$. Under these assumptions a velocity potential $\Phi = \Phi(r, \theta, z, t)$ exists which we approximate in this paper using the modified mild-slope equation (derived in Chamberlain & Porter 1995).

We therefore have

$$\Phi(r, \theta, z, t) \approx \phi(r, \theta) \frac{\cosh k(z + h)}{\cosh kh} \mathrm{e}^{-\mathrm{i}\sigma t}, \tag{2.1}$$

where $\phi = \phi(r, \theta)$ satisfies

$$\nabla \cdot (u \nabla \phi) + v\phi = 0 \quad (0 < r, \quad 0 \leqslant \theta < 2\pi), \tag{2.2}$$

in which $\nabla = (\partial/\partial r, \partial/r\partial\theta)$ and

$$v = k^2 u + u_1 \nabla^2 h + u_2 (\nabla h)^2, \tag{2.3}$$

$u > 0$, u_1 and u_2 being functions of h, which are given by

$$u = \frac{1}{2k} \tanh(kh) \left(1 + \frac{K}{\sinh K} \right),$$

$$u_1 = \frac{\operatorname{sech}^2(kh)}{4(K + \sinh(K))} \{ \sinh(K) - K \cosh(K) \},$$

$$u_2 = \frac{k\operatorname{sech}^2(kh)}{12(K+\sinh(K))^3}\left\{K^4 + 4K^3\sinh(K) - 9\sinh(K)\sinh(2K)\right.$$
$$\left. + 3K(K+2\sinh(K))(\cosh^2(K) - 2\cosh(K) + 3)\right\},$$

in which $K = 2kh$. The angular frequency $\sigma > 0$ is assumed given and the local wavenumber $k = k(h)$ is the positive real root of the dispersion relation

$$\nu \equiv \frac{\sigma^2}{g} = k\tanh kh \tag{2.4}$$

at each point (r, θ). In any region where h is a constant, the functions u and v occurring in (2.2) are also constant and satisfy $v = k^2u$, where k denotes the appropriate solution of the dispersion relation. The approximation to the free-surface elevation corresponding to (2.1) is

$$\eta(r,\theta,t) \approx \operatorname{Re}\left\{\frac{-\mathrm{i}\sigma\phi(r,\theta)}{g}\right\}.$$

The derivation of (2.2) with (2.3) supposes that the topography satisfies the mild-slope assumption, that $|\nabla h|/kh = O(\varepsilon)$, where $\varepsilon \ll 1$. The simpler but less accurate mild-slope equation, due originally to Berkhoff (1973, 1976), is given by retaining only the first term on the right-hand side of (2.3). A further simplification arises in the long wave case $kh \ll 1$, when (2.2) reduces to the corresponding shallow water equation in which $u = h$ and $v = \nu$.

We now suppose that the depth profile is axisymmetric so that $h = h(r)$, which is assumed to be a continuous function. (Although the depth is required to be a slowly varying function, there is no advantage to be gained by writing $h = H(\varepsilon r)$.) It follows that (2.2) may be written as

$$\frac{1}{r}(ur\phi_r)_r + \frac{u}{r^2}\phi_{\theta\theta} + v\phi = 0 \quad (0 < r, \quad 0 \leqslant \theta < 2\pi) \tag{2.5}$$

and that (2.3) reduces to

$$v = k^2u + u_1(h'' + h'/r) + u_2h'^2,$$

so that the term involving u_1 actually contains an $O(\varepsilon)$ correction to the mild-slope equation. We further suppose that

$$h(r) = \begin{cases} h_a & (0 \leqslant r \leqslant a), \\ h_b & (b \leqslant r), \end{cases} \tag{2.6}$$

where $0 \leqslant a < b$, h_a and h_b being constants, and for notational convenience we write $k_a = k(h_a)$ and $k_b = k(h_b)$. We allow $h'(r)$ to be discontinuous at $r = a$ and at $r = b$.

Let an incident wave ϕ_I, with real amplitude I, be represented in $r > b$ by

$$\phi_I = I\mathrm{e}^{\mathrm{i}k_br\cos\theta}$$
$$= I\left(J_0(k_br) + 2\sum_{m=1}^{\infty}\mathrm{i}^mJ_m(k_br)\cos m\theta\right) \tag{2.7}$$

and write $\phi = \phi_I + \phi_S$ where ϕ_S represents the waves scattered by the topography and satisfies the radiation condition

$$r^{1/2}\left(\frac{\partial\phi_S}{\partial r} - \mathrm{i}k_b\phi_S\right) \to 0, \quad r \to \infty \tag{2.8}$$

uniformly in θ.

By hypothesis, u and v are both constants for $r > b$ and $v = k_b^2 u$. Hence (2.5) simplifies to

$$r(r\phi_r)_r + \phi_{\theta\theta} + k_b^2 r^2 \phi = 0 \quad (b < r, \quad 0 \leqslant \theta \leqslant 2\pi)$$

and we take the scattered wave solution in the form

$$\phi_S(r,\theta) = B_0 H_0^{(1)}(k_b r) + 2\sum_{m=1}^{\infty} \mathrm{i}^m B_m H_m^{(1)}(k_b r)\cos m\theta, \quad (b \leqslant r, \quad 0 \leqslant \theta \leqslant 2\pi), \tag{2.9}$$

which satisfies the radiation condition (2.8). The coefficients B_m, $m = 0, 1, 2, \ldots$ must be found as part of the solution procedure.

We similarly find that, for $0 \leqslant r \leqslant a$, the total solution for ϕ may be written as

$$\phi(r,\theta) = A_0 J_0(k_a r) + 2\sum_{m=1}^{\infty} \mathrm{i}^m A_m J_m(k_a r)\cos m\theta, \quad (0 \leqslant r \leqslant a, \quad 0 \leqslant \theta \leqslant 2\pi), \tag{2.10}$$

for some coefficients A_m, the Bessel functions which are unbounded at $r = 0$ having been discarded.

The core of the problem is now clear. We have to solve (2.5) for $a < r < b$, $0 \leqslant \theta \leqslant 2\pi$, matching its solution with the version of ϕ given by (2.10) at $r = a$ and with $\phi = \phi_I + \phi_S$, given by (2.7) and (2.9), at $r = b$. This matching process will ultimately determine the coefficients A_m and B_m.

At $r = a$ and $r = b$ we obviously require continuity of ϕ, to ensure continuity of the free-surface elevation. A further condition at these junctions is implied by a consistent application of (2.5) there and this leads to the interfacial condition

$$u(h)[\phi_r(r,\theta)] + u_1(h)\phi(r,\theta)[h'(r)] = 0, \tag{2.11}$$

where $[\cdot]$ denotes the jump in the enclosed quantity. Porter & Staziker (1995) have shown, for general topography, that the condition (2.11) represents conservation of mass at locations where the bed slope is discontinuous.

On the basis of these remarks, the overall matching conditions to be applied at $r = a$ and $r = b$ are

$$\left.\begin{aligned} \phi(a-,\theta) &= \phi(a+,\theta), \\ \phi(b-,\theta) &= \phi(b+,\theta), \\ \phi_r(a-,\theta) - \phi_r(a+,\theta) &= \mu_a \phi(\pm a,\theta), \\ \phi_r(b-,\theta) - \phi_r(b+,\theta) &= -\mu_b \phi(\pm b,\theta), \end{aligned}\right\} \tag{2.12}$$

where

$$\mu_a = u_1(h_a)h'(a+)/u(h_a), \quad \mu_b = u_1(h_b)h'(b-)/u(h_b).$$

The condition (2.11) also has to be applied at other locations where h' is discontinuous, although we do not consider such topography here. In view of (2.7), (2.9) and (2.10) we seek a solution ϕ for $a < r < b$, $0 \leqslant \theta \leqslant 2\pi$ in the form

$$\phi(r,\theta) = \rho_0(r) + 2\sum_{m=1}^{\infty} \mathrm{i}^m \rho_m(r)\cos m\theta. \tag{2.13}$$

It follows from (2.5) that

$$L(\rho_m) \equiv r(ru\rho_m')' + (r^2 v - m^2 u)\rho_m = 0 \quad (a < r < b), \tag{2.14}$$

for $m = 0, 1, 2\ldots$, and from (2.9), (2.10) and (2.12) that

$$\left.\begin{aligned} A_m J_m(k_a a) &= \rho_m(a), \\ k_a A_m J'_m(k_a a) &= \rho'_m(a) + \mu_a \rho_m(a), \\ I J_m(k_b b) + B_m H^{(1)}_m(k_b b) &= \rho_m(b), \\ I k_b J'_m(k_b b) + k_b B_m H^{(1)\prime}_m(k_b b) &= \rho'_m(b) + \mu_b \rho_m(b), \end{aligned}\right\} \tag{2.15}$$

also for $m = 0, 1, 2\ldots$. Eliminating A_m and B_m we obtain mixed boundary conditions for (2.14) in the form

$$\left.\begin{aligned} J_m(k_a a)\rho'_m(a) + (\mu_a J_m(k_a a) - k_a J'_m(k_a a))\rho_m(a) &= 0, \\ H^{(1)}_m(k_b b)\rho'_m(b) + (\mu_b H^{(1)}_m(k_b b) - k_b H^{(1)\prime}_m(k_b b))\rho_m(b) &= \frac{-2\mathrm{i}I}{b\pi}, \end{aligned}\right\} \tag{2.16}$$

for $m = 0, 1, 2\ldots$, the Wronskian $J'_m(x)H^{(1)}_m(x) - J_m(x)H^{(1)\prime}_m(x) = -2\mathrm{i}/x\pi$ having been used to simplify the condition at $r = b$.

The solution of the scattering problem is therefore determined, in principle, by solving the boundary value problem consisting of (2.14) and (2.16) for the complex-valued functions ρ_m, for each m, following which the values of A_m and B_m can be recovered from (2.15). However, from a practical point of view it is clearly more convenient to deal with a real-valued problem. To achieve this we denote by $R_m(r)$ the radial component of the mth mode, defined so that

$$\phi(r, \theta) = A_0 R_0(r) + 2\sum_{m=1}^{\infty} \mathrm{i}^m A_m R_m(r) \cos m\theta \quad (0 \leqslant r, 0 \leqslant \theta \leqslant 2\pi) \tag{2.17}$$

and we note that this implies

$$\rho_m(r) = A_m R_m(r) \quad (a \leqslant r \leqslant b).$$

Also,

$$R_m(r) = J_m(k_a r) \quad (0 \leqslant r \leqslant a) \tag{2.18}$$

and we can therefore determine R_m over the varying topography by means of the real initial value problem

$$\left.\begin{aligned} L(R_m) &= 0 \qquad\qquad (a < r < b), \\ R_m(a) &= J_m(k_a a), \\ R'_m(a) &= k_a J'_m(k_a a) - \mu_a J_m(k_a a). \end{aligned}\right\} \tag{2.19}$$

The coefficients A_m and B_m are found in terms of R_m by enforcing the boundary conditions at $r = b$ in (2.15) and (2.16), leading to

$$A_m = 2\mathrm{i}I/\pi b\alpha_m, \quad B_m = -I\,\mathrm{Re}\,(\alpha_m)/\alpha_m, \tag{2.20}$$

in which

$$\alpha_m = \left(k_b H^{(1)\prime}_m(k_b b) - \mu_b H^{(1)}_m(k_b b)\right) R_m(b) - H^{(1)}_m(k_b b) R'_m(b). \tag{2.21}$$

We deduce from (2.20) that $I \neq 0$ implies $|A_m| > 0$ and that

$$\left.\begin{aligned} \mathrm{i}B_m/A_m &= -\tfrac{1}{2} b\pi \mathrm{Re}\,(\alpha_m) = I\,\mathrm{Im}\,(1/A_m) \\ (I + B_m)/A_m &= \tfrac{1}{2} b\pi \mathrm{Im}\,(\alpha_m) = I\,\mathrm{Re}\,(1/A_m) \end{aligned}\right\} (m = 0, 1, 2\ldots). \tag{2.22}$$

The scattering problem is now resolved through the initial value problem (2.19) but we can complete the specification of R_m by comparing (2.17) with (2.7) and (2.9) and use (2.22) to show that

$$R_m(r) = -\tfrac{1}{2}b\pi \mathrm{Im}\,(\bar{\alpha}_m H_m^{(1)}(k_b r)) = I\,\mathrm{Re}\,(H_m^{(1)}(k_b r)/\overline{A}_m) \quad (r \geqslant b)$$
$$\sim I(2/\pi k_b r)^{1/2} \cos\,(k_b r - \tfrac{1}{2}m\pi - \tfrac{1}{4}\pi + \arg\,(A_m))/|A_m| \quad r \to \infty. \qquad (2.23)$$

We have tacitly assumed that $\alpha_m \neq 0$ for every m in the above expressions and we now confirm that this is indeed the case. Suppose that $\alpha_m = 0$. Then $\mathrm{Re}(\alpha_m)$ and $\mathrm{Im}(\alpha_m)$ are both zero, a fact which may be written in the form

$$\begin{pmatrix} k_b J_m'(k_b b) - \mu_b J_m(k_b b) & -J_m(k_b b) \\ k_b Y_m'(k_b b) - \mu_b Y_m(k_b b) & -Y_m(k_b b) \end{pmatrix} \begin{pmatrix} R_m(b) \\ R_m'(b) \end{pmatrix} = \begin{pmatrix} 0 \\ 0 \end{pmatrix}.$$

The determinant of the above matrix is

$$\left(\mu_b J_m(k_b b) - k_b J_m'(k_b b)\right) Y_m(k_b b) - \left(\mu_b Y_m(k_b b) - k_b Y_m'(k_b b)\right) J_m(k_b b) = 2/b\pi$$

(using the Wronskian of J_m and Y_m) and, since this is non-zero, it follows that $R_m(b) = R_m'(b) = 0$ which is a contradiction as R_m solves the initial value problem (2.19). It follows that $\alpha_m \neq 0$.

It is anticipated that the scattered wave will be dominated by the leading modes and that a good approximation to the solution can be obtained by solving (2.19) for $m = 0, 1, 2 \ldots, M$, for a relatively small value of M. This is indeed the case, in general, although there are exceptions as we indicate in § 3, where typical numerical results are given.

Finally in this section we describe how the approach described above can be applied to a slightly different problem. We suppose that a circular island in the form of a surface-piercing circular cylinder is present in $r < a$ with the region of varying h in $a < r < b$ describing a submerged shoal. The appropriate boundary condition at $r = a$ is $\phi_r(a+, \theta) = 0$ and, again using (2.13), we therefore replace the first two equations in (2.15) with $\rho_m'(a) = 0$. The matching and boundary conditions at $r = b$ remain unchanged. We again seek the solutions ρ_m in the form $\rho_m(r) = A_m R_m(r)$ where the real-valued function R_m satisfies $L(R_m) = 0$ in $r > a$ subject to the initial conditions $R_m(a) = 1$, $R_m'(a) = 0$. It is readily seen that the boundary condition at $r = b$ implies that A_m and B_m are again given by the expressions in (2.20).

3. The scattering problem

In this section we present a number of results determined by a numerical implementation of the methods described in § 2. (For the purposes of all scattering problems considered we set $I = 1$.) The formulation adopted has the consequence that the only significant numerical effort required is in solving the initial value problem (2.19) (or the version with simpler initial conditions for a surface-piercing island). This is a routine problem to which we have applied a standard error-checking Runge–Kutta method (see Lambert 1992, for example).

One of our purposes is to show that accurate results can generally be achieved by using only very few modes, that is, by approximating (2.17) by

$$\phi(r, \theta) = A_0 R_0(r) + 2\sum_{m=1}^{M} \mathrm{i}^m A_m R_m(r) \cos\,(m\theta) \quad (0 < r, \quad 0 \leqslant \theta \leqslant 2\pi) \qquad (3.1)$$

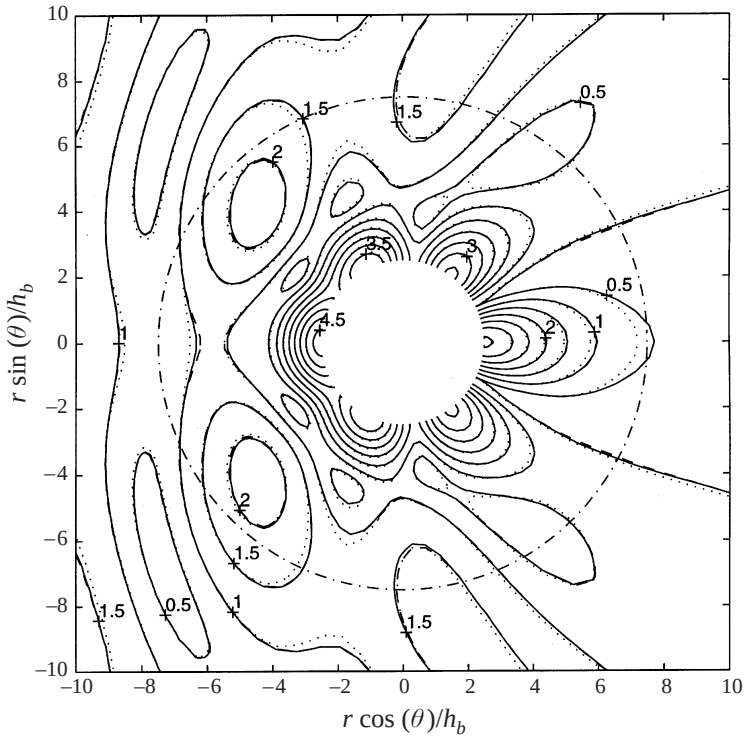

FIGURE 1. Contour plots of $|\phi_I + \phi_S|$ showing the scattering effects of the circular island. Three sets of results are presented each corresponding to a different value of M in (3.1): dotted to $M = 4$, broken to $M = 5$ and solid to $M = 6$.

for a relatively small value of M. We note that in the case discussed at the end of § 2 of a surface-piercing island we must replace $0 < r$ with $a < r$ in the above expression.

We begin by considering a problem for which numerical results have already been determined by other authors.

3.1. *Surface-piercing islands*

Xu & Panchang (1993) considered wave scattering by a circular island using a direct numerical approach to approximate the solution of the mild-slope equation. The island is of radius 10 km with a shoal in the form $h(r) = \alpha r^2$ adjoining a constant depth of 4 km at all horizontal locations greater than 30 km from the centre of the island. The constant α is fixed by the fact that the still-water depth nearest the island is 444 m. Xu & Panchang presented results for three different wave periods and here we examine the smallest wave period of 240 s, this being the case that is numerically the most demanding.

When we convert the data given in the preceding paragraph into the notation of the present paper and non-dimensionalize with respect to h_b, we find that

$$a/h_b = 2.50, \quad b/h_b = 7.50, \quad h_a/h_b = 0.111 \quad \text{and} \quad \nu h_b = 0.280,$$

from which it follows that $\alpha h_b = 0.0178$. Here three significant figures have been given throughout.

In figure 1 contour plots of $|\phi_I + \phi_S|$, which is proportional to the absolute free-surface elevation, are shown, the 'dash-dot' line indicating the position of the outer

extent of the shoal. Three sets of contour lines are given, for three different values of M in (3.1): the dotted contours correspond to $M = 4$, the dashed contours to $M = 5$ and the solid contours to $M = 6$. The corresponding contour lines for $M \geqslant 7$ are indistinguishable from those with $M = 6$. A comparison of these graphical results and those given by Xu & Panchang shows good agreement. It is interesting to note that their contours near the 'footprint' shapes towards the right-hand side of the figure closely resemble those corresponding to truncation at $M = 4$ in the present calculation. This may be due to Xu & Panchang's use of a fairly coarse numerical mesh which evidently does not resolve the contributions from the higher angular modes.

Zhu & Zhang (1996) have also considered scattering by a circular island. In their study there is a conical shoal of the form $h(r) = \gamma r$ $(a \leqslant r \leqslant b)$, in which γ is a constant, surmounted by a circular cylinder; this special bed shape permits an analytic solution in the shallow water limit. Most of Zu & Zhang's paper is concerned with using this analytic solution to validate a numerical integration of the mild-slope equation. We have not been able to agree with all of the results which they present for the mild-slope approximation. For example, in their figure 5 a comparison of wave run-up at the island is presented for both the shallow water and mild-slope approximations; we can reproduce their analytic results using our approximation scheme (replacing u with h and $\tanh(kh)$ with its argument in the dispersion relation (2.4)) but the curve we obtain for the mild-slope approximation is rather different to theirs; in particular our version of this curve has a continuous slope and predicts smaller run-up than the shallow water approximation at all points around the island.

3.2. *Submerged topography*

Here we consider a particular example of a topography that is completely submerged, given by

$$h(r) = \tfrac{1}{2}\left(h_a + h_b - (h_b - h_a)\cos((r-a)/(b-a)\pi)\right) \quad (a \leqslant r \leqslant b)$$

which represents a smooth join from the depth h_a in $r < a$ to the depth h_b in $r > b$. We shall return to this particular example several times to illustrate different issues. Here, we consider the specific case where $a/h_b = 4$ (the dimensionless radius of the central plateau), $b/h_b = 5$ (the dimensionless outer radius of the varying depth region) and $h_a/h_b = 1/16$, for four different incident wave frequencies.

Numerical results presented in this subsection are all based on the solution truncated at $M = 8$; larger values of M do not make any discernible differences to graphical results.

In figure 2 contour plots are shown of $|\phi_I + \phi_S|$ for the four different frequencies. (In the interests of economy we have exploited symmetry in the problem and presented results for $0 \leqslant \theta \leqslant \pi$ only.) In plot (*a*), corresponding to $\nu h_b = 0.25$, it is clear how the incident wave is deformed by the presence of the bed irregularity. The contour lines indicate integer values of $|\phi_I + \phi_S|$ from 1 to 9 ($\max(|\phi_I + \phi_S| \approx 9.6$ in this case). Plots (*b–d*) present similar information, but for increasingly large frequencies. In each case the contours correspond to integer values of $|\phi_I + \phi_S|$ and the maximum values of this quantity are approximately 13.0, 9.3 and 7.1 for $\nu h_b = 0.5, 0.75$ and 1 respectively.

We note that in the plot corresponding to $\nu h_b = 0.5$ there is evidence of the near-resonance which has been observed in related problems before. Evidently, this is an example for which the fifth mode dominates with $|A_5|$ taking a relatively large value. We explore this issue in the following section.

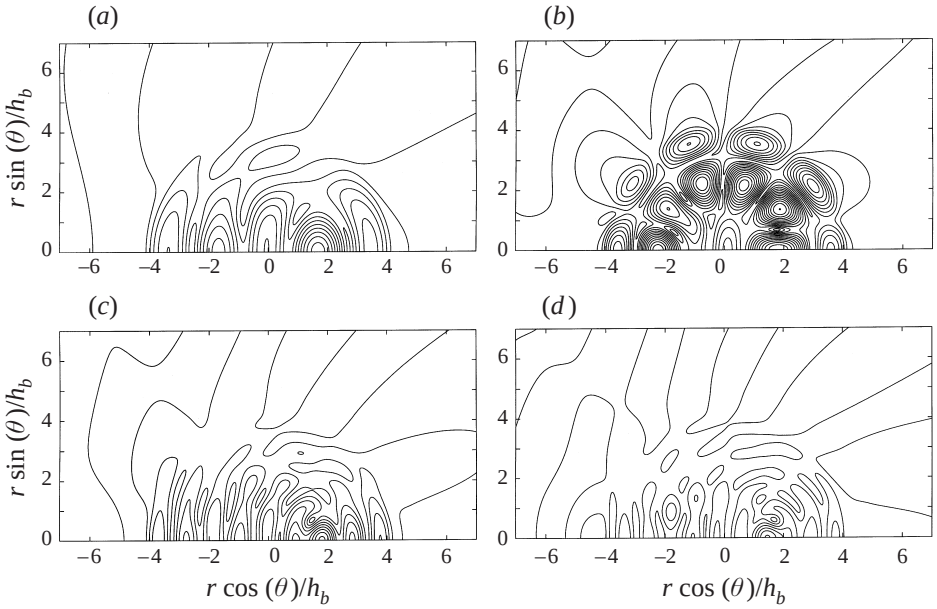

FIGURE 2. Contour plots of $|\phi_I + \phi_S|$ for the submerged topography for four different wave frequencies: (*a*) $\nu h_b = 0.25$, (*b*) 0.5, (*c*) 0.75, (*d*) 1.0. In each plot there are 10 contour lines at heights equally spaced between 0 and $\max(|\phi_I + \phi_S|)$.

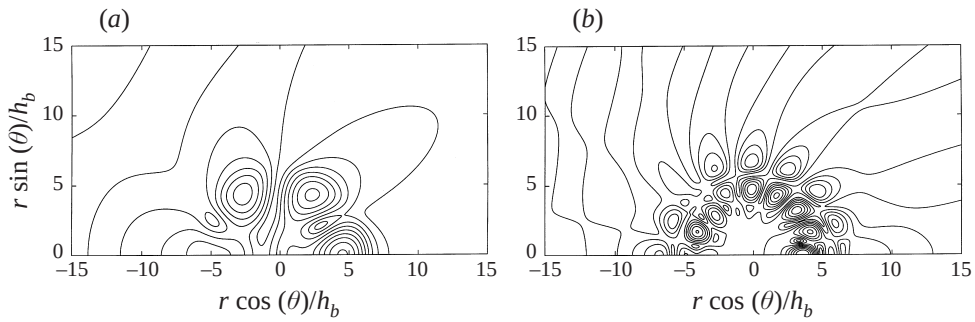

FIGURE 3. Contour plots of $|\phi_I + \phi_S|$ for waves of two particular frequencies, (*a*) $\nu h_b = 0.0715$, (*b*) 0.466, incident on a submerged island.

4. Near-resonance and near-trapping

If the topography is assigned, the only free parameters in the problem are the frequency σ and the incident wave amplitude I. A trapped wave corresponds to a non-trivial solution of the unforced problem with $I = 0$, for some value of the frequency. Such a wave is represented by a non-trivial solution of (2.5) and (2.12) with $I = 0$ and it easily follows that such a solution exists if and only if $\alpha_m = 0$ for some $m = 0, 1, 2, \ldots$ and some real value of $\nu = \sigma^2/g$, which can be regarded as an eigenvalue parameter. We have already shown in § 2 that this is not possible and therefore the topography considered cannot support trapped waves. Equivalently, resonance is not possible in the scattering problem as A_m is bounded for all m and all real values of ν.

However, as we have already noted, the results of numerical experiments indicate

that at certain frequencies the free-surface elevation over raised topography can become extremely large, to the extent that the scattered wave field there completely dominates the wave field over the outer horizontal bed. This situation is typified by figure 2(*b*) and is not unusual. In figure 3 we again consider the depth profile h defined in § 3.2 but now with the different dimensionless parameters $a/h_b = 6$, $b/h_b = 10$ and $h_a/h_b = 0.1$. In each case the contour lines show integer values of $|\phi_I + \phi_S|$ up to a maximum value of 9. Figure 3(*a*) corresponds to $\nu h_b = 0.0715$ and it is clear that the $m = 3$ mode is particularly significant; figure 3(*b*), which is for $\nu h_b = 0.466$, shows an example in which the $m = 8$ mode dominates. In each of these cases, the pronounced angular periodicity of the free-surface contour plot identifies the particular mode which is responsible for the large amplitudes. Thus a particular coefficient A_m, although bounded, can become large (relative to I) at one or more frequencies. Reference to (2.20) shows that the corresponding $|\alpha_m| \ll 1$ and that $|B_m/A_m| \ll 1$ at such frequencies, from which it follows that $|R_m(b)| \ll 1$ and $|R_m'(b)| \ll 1$. The solution for R_m must therefore decrease in magnitude in (a, b), and do so rapidly, at certain frequencies.

To gain some insight into this phenomenon, which we have described as near-resonance in § 1, we can examine the solutions of the scattering problem in the phase-plane (more information concerning phase-planes may be found in Jordan & Smith 1977, for example). For current purposes we shall suppose that $m \geqslant 1$; the $m = 0$ case is discussed at the end of this subsection. We thus replace (2.19) by the first-order system

$$\left.\begin{aligned} ruR_m' &= S_m, \quad S_m' = -(r^2\nu - m^2 u)R_m/r \quad (r > a), \\ R_m(a) &= J_m(k_a a), \\ S_m(a) &= \{k_a J_m'(k_a a) - \mu_a J_m(k_a a)\}/au_a, \end{aligned}\right\} \tag{4.1}$$

where $u_a = u(h(a))$. In the (R_m, S_m)-plane the coupled equations give rise to saddle-like behaviour, corresponding to a monotonic free-surface profile, if $r^2\nu - m^2 u < 0$, and focal- or spiral-like behaviour, corresponding to an oscillatory free-surface profile, if $r^2\nu - m^2 u > 0$. Moreover, in the case of the saddle, R_m and S_m have decreasing magnitudes in the quadrants in which they have opposite signs and we infer that the part of the phase-plane trajectory corresponding to near-resonance lies in one of these quadrants.

The coefficient $P = (r^2\nu - m^2 u)/r$ which determines the behaviour of the solution of (4.1) is given by $P = u(r^2k^2 - m^2)/r$ when the mild-slope equation is substituted for (2.2), and this provides a simple explicit form from which to determine the overall qualitative behaviour. The sign of P can be determined in this simpler case by plotting $k(r)$ against m/r for $r > 0$. Since each continuous function $h(r)$ leads to a continuous function $k(r)$, by (2.4), with $k = k_a$ for $0 \leqslant r \leqslant a$ and $k = k_b$ for $b \leqslant r$, it is clear from this construction that $P(r)$ will have an odd number of zeros in $r > 0$, for each m. Figure 4 illustrates the situation for the case in which $h(r)$ is a smooth function which is increasing for $a < r < b$, and with $a = 4h_b$ and $b = 10h_b$.

Referring to figure 4 (in which we have only shown curves for $m = 2, 4$ and 6, for clarity) and noting (2.18), we infer the following. For each m, the phase path transfers from growing saddle-like behaviour with $P < 0$ to spiral-like behaviour with $P > 0$, either directly (if P has only one zero) or ultimately (if P has three zeros). For $m = 1$ and $m \geqslant 7$, this transfer is direct and occurs at a value $r < a$ for $m = 1$ and a value $r \gg b$ for $m \geqslant 7$. For the remaining values of m, P has three zeros and the phase paths exhibit an intermediate spiral-like behaviour ($P > 0$) and a further

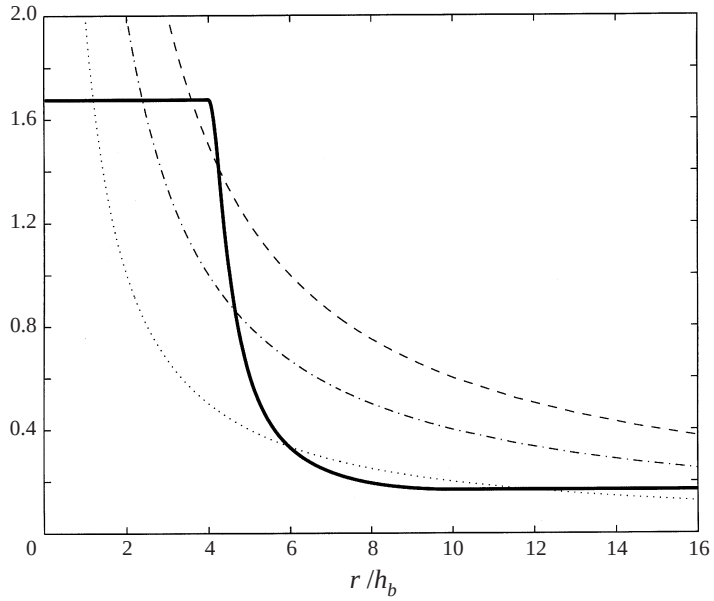

FIGURE 4. A typical example of $k = k(r)$ for a smoothly increasing function h. The broken lines show m/r for three different values of m: $\cdots\cdots$, $m = 2$; $-\cdot-\cdot-$, $m = 4$; $- - - -$, $m = 6$.

saddle-like behaviour ($P < 0$) before attaining the final spiral state in $r > b$. The additional saddle behaviour is necessary to produce the rapid decay in $R_m(r)$ required for near-resonance.

Although the cases $2 \leqslant m \leqslant 6$ have the same characteristics according to figure 4, they give rise to quite different phase paths, as figure 5 reveals. The phase paths are shown in the (R_m, R'_m)-plane, rather than the (R_m, S_m)-plane, as these are more informative and, in particular, allow direct connections to be made with (2.18) and (2.23). The use of $R'_m = S_m/ru$ in place of S_m has an inevitable distorting effect, but the qualitative properties deduced above are nevertheless clearly evident in figure 5. The intermediate saddle-like behaviour occurs in either the second or fourth quadrant in each case, as anticipated, but only for $m = 4$ is there strong decay corresponding to near-resonance. What distinguishes this case is that part of the saddle trajectory coincides with the stable manifold, a fact which can be confirmed numerically by slightly de-tuning the near-resonant frequency.

As for the other two displayed cases, we note that R'_2 has a relatively small value when the final spiral is attained but R_2 has not; and that the scale of the phase portrait for $m = 6$ is consistent with A_6 being relatively small and therefore with the fact that we expect the higher-order modes to contribute little to the overall solution of the scattering problem, apart from in the exceptional cases of near-resonance.

We can in fact distinguish the modes $m = 2, 4, 6$ in terms of $j_{m,p}$ and $j'_{m,p}$, which denote the pth zeros ($p = 1, 2, 3\ldots$) of $J_m(x)$ and $J'_m(x)$, respectively, ordered so that $j_{m,p+1} < j_{m,p}$ and $j'_{m,p+1} < j'_{m,p}$. These zeros satisfy $j_{m,1} > j'_{m,1} > m$ and $j'_{m,p+1} > j_{m,p} > j'_{m,p}$. We find that, for the parameter values used in figure 4, $2 < j'_{2,2} < ak_a < j_{2,2}, 4 < j'_{4,1} < ak_a < j_{4,1}$ and $ak_a < 6 < j'_{6,1} < j_{6,1}$. More generally, the condition $j'_{m,p} < ak_a < j_{m,p}$ is necessary for near-resonance. The case $m = 2$ above shows that it is not sufficient.

The further phase portraits in figure 6 show the effect of varying v, for a fixed

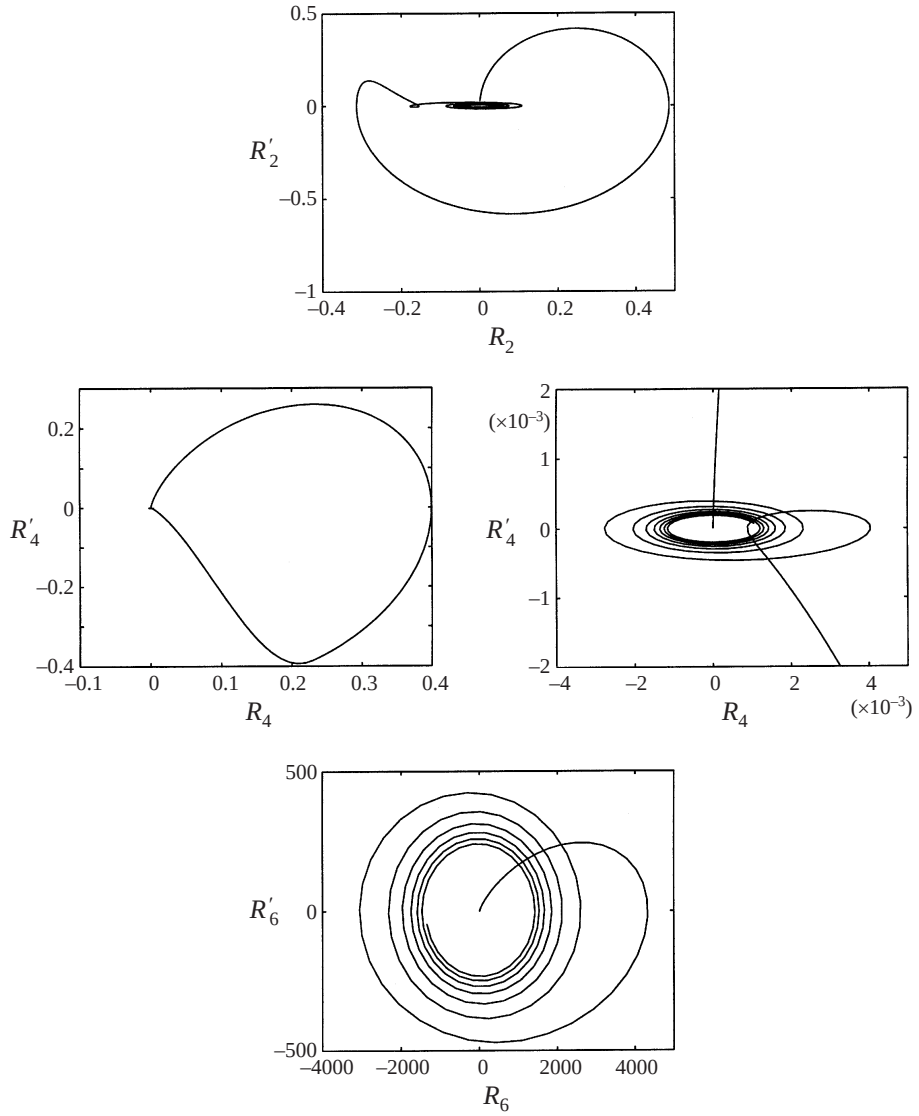

FIGURE 5. Plots of R_m against R_m' for the three values of m examined in figure 4 and for a finite range of the independent variable r. In the case of R_4 in which $R_4(b)$ and $R_4'(b)$ are both small a second plot alongside shows the detail near the origin.

topography and a fixed value of m. The topography considered here is defined by

$$h(r) = h_a - (h_a - h_b)\,\frac{\tilde{r}^2(3\tilde{r}^2 - 4(1+\alpha)\tilde{r} + 6\alpha)}{2\alpha - 1}$$

in which $\tilde{r} = (r-a)/(b-a)$ and we choose $\alpha = 0.26$, $a/h_b = 5$, $b/h_b = 7$ and $h_a/h_b = 0.1$; this bed shape may be thought of as a submerged crater with a raised lip. It follows from (2.4) that $k(r)$ is a continuous, increasing function of v at each r. Therefore, for a fixed topography, the values of r at which P changes sign vary continuously with v for each m, and we can locate those frequencies which correspond to near-resonance, in each mode. Figure 6 shows $|A_4|$ for the test topography, together with the graphs

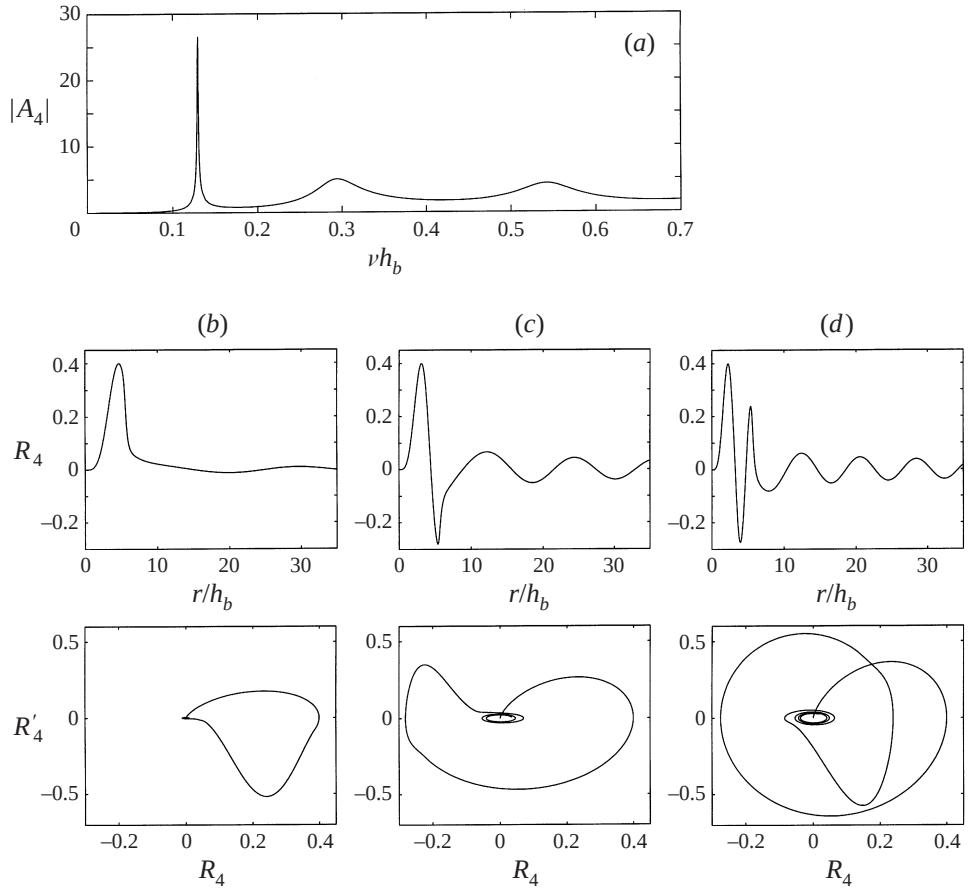

FIGURE 6. (*a*) $|A_4|$ plotted against νh_b for the topography described in the text. The three pairs of plots below are for those νh_b corresponding to local maxima of $|A_4|$, (*b*) $\nu h_b = 0.1294$, (*c*) 0.2921, (*d*) 0.5465, and show R_4 plotted against r/h_b and also in a phase portrait against R_4'.

of R_4 and the phase plots at the frequencies corresponding to three successive local maxima in $|A_4|$; in each case, to aid clarity, only the first few oscillations for the solution in $r > b$ are shown. Each successive local maximum is associated with an extension of the intermediate spiral in the phase path by a further half-circuit of the origin, resulting in an additional oscillation in R_4. The height of the successive local maxima correspondingly decrease and pronounced near-resonance arises when the phase path transfers to the stable manifold at an early opportunity. In the case shown in figure 6 only a transfer at the first such opportunity corresponds to significant near-resonance.

Near-resonance can also occur in the $m = 0$ mode. However the discussion concerning zeros of Bessel functions takes a slightly different form. Once again we use $j_{0,p}$ to denote the pth positive zero of J_0 but it is convenient to use $j'_{0,p}$ as the pth *non-negative* zero of J_0' (so that $j'_{0,0} = 0$ and $j'_{0,p} = j_{1,p-1}$ $(p > 0)$). It follows that $j'_{0,p} < j_{0,p}$ and resonance can occur when $j'_{0,p} < ak_a < j_{0,p}$ these being the situations when the trajectory corresponding to (4.1) approaches the origin in the second or fourth quadrants.

4.1. *Near-trapping*

A different interpretation of the phenomenon of near-resonance is that the homogeneous problem with $I = 0$ has eigenvalues $\nu \in \mathbb{C}$ which have small but non-zero imaginary parts. Such eigenvalues imply complex frequencies and reference to (2.1) shows that $\mathrm{Im}(\sigma) < 0$ corresponds to waves which decay with time. We can therefore seek those eigenvalues ν of the homogeneous problem which have small imaginary parts and refer to the associated transient wave solutions as 'nearly trapped waves', when $\mathrm{Im}(\nu) < 0$.

We thus consider the homogeneous version of (2.20) arranged in the form $\alpha_m(\nu)A_m = 0$ and $\alpha_m(\nu)B_m = 0$, and solve the eigenvalue equations $\alpha_m(\nu) = 0$ with $\nu \in \mathbb{C}$ and for a range of values of m, noting that $k \in \mathbb{C}$ is induced by (2.4). The free-surface elevation corresponding to a root of $\alpha_m(\nu) = 0$ can be determined from the (now complex-valued) function $R_m(r)$, using $A_m = 1$ to normalize the solution and choosing B_m to ensure continuity at $r = b$. Thus the eigenfunction is given by (2.18) for $0 < r < a$, by (2.19) for $a \leqslant r \leqslant b$ and by

$$R_m(r) = R_m(b)H_m^{(1)}(k_b r)/H_m^{(1)}(k_b b)$$

for $b \leqslant r$, in which $R_m(b)$ is determined by (2.19).

The numerical approach we adopt to identify the complex roots of $\alpha_m(\nu) = 0$ is to use an approximate version of Newton's method in the form

$$\nu_{n+1} = \nu_n - \alpha_m(\nu_n) \Bigg/ \left(\frac{\alpha_m(\nu_n + \delta) - \alpha_m(\nu_n)}{\delta} \right), \qquad n = 0, 1, 2, \ldots,$$

beginning with some value ν_0. Here δ is chosen to be small ($\delta = 10^{-5}$ was used in all of the numerical results given below); the use of a one-sided difference to approximate the derivative reduces the number of evaluations of α_m when compared with a central difference approximation.

Let us now return to the example encountered in § 3 of a submerged island with a cosine-shaped shoal. In that example we found that for $\nu h_b = 0.5$ the scattered wave was dominated by the fifth mode. Putting $m = 5$ and adopting the procedure described above we find that the zeros of α_5, scaled with respect to h_b and with $\mathrm{Re}\,(\nu h_b) \in (0, 2)$ are: $0.259808 - 0.000065\mathrm{i}$, $0.494593 - 0.004471\mathrm{i}$, $0.746358 - 0.057433\mathrm{i}$, $0.956129 - 0.144069\mathrm{i}$, $1.289657 - 0.117206\mathrm{i}$ and $1.743695 - 0.117824\mathrm{i}$ where six decimal places have been given.

We can obtain still more information about this problem by considering A_5 for a range of νh_b. Figure 7 shows a graph of $|A_5|$ against νh_b with a logarithmic axis for $|A_5|$. Two large peaks are apparent and are shown in more detail in plots (*b*) and (*c*), in which a dotted vertical line indicates the position of the real part of the nearest zero of α_5. In general a local maximum of $|A_m|$ will not occur at a value of νh_b which is exactly equal to the real part of a zero of α_m. However, for pronounced near-resonance, the imaginary part of the zero of α_m is so small that the stationary point and the real part of a zero almost coincide; for weaker near-resonance, the values are more obviously distinct.

We notice that there is a zero of α_5 near $\nu h_b = 0.25$ but, unlike the zero near $\nu h_b = 0.5$, this was not evident in figure 2. Figure 7 indicates why this is the case: the large peak near $\nu h_b = 0.25$ is much more narrow than any of the other peaks and is consequently a more finely-tuned phenomenon. We have found this property to be typical, with the highest peaks of $|A_m|$ having the narrowest bandwidth.

If we choose $\nu h_b = 0.259808$ we expect that the corresponding scattered wave

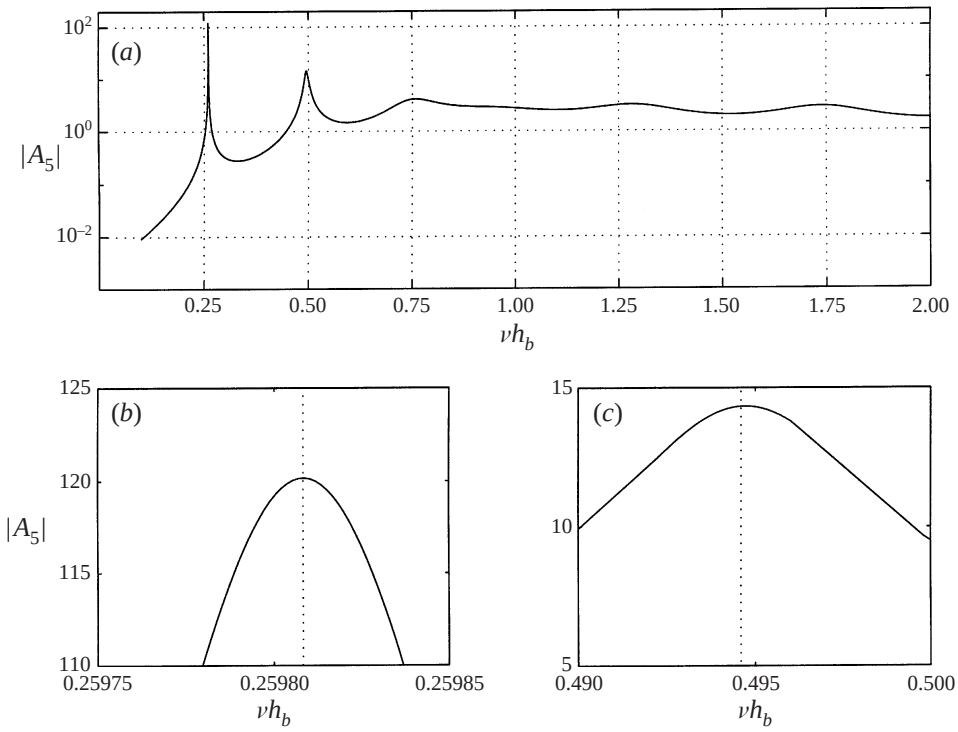

FIGURE 7. The graph at the top shows $|A_5|$ plotted against the dimensionless deep water wavenumber νh_b. The two plots below show close-ups of the first two local maxima of $|A_5|$; the dotted lines indicate the position of the real part of a zero of α_5.

will be entirely dominated by the fifth mode. This is indeed the case as we see in figure 8 in which Re $(\phi_I + \phi_S)$ is shown as a surface plot. This plot *is* dominated by the fifth mode to the extent that all other features are indistinguishable. In fact $\max(\phi_S/I) > 92$ in this case.

The results we present in what follows are typical of extensive numerical experiments that have been carried out. For the purposes of this study we return to the submerged 'cosine-shoal' island first defined in § 3.2 and examine near-resonance. The concept of near-trapping as described above provides a convenient means by which we can carry out this procedure. In the first study we monitor how the zeros of α_6 move in the complex plane as a result of changing one particular parameter.

We begin by examining how the depth over a relatively shallow central section affects the position of the zero of α_6 having the smallest positive real part (that is, the zero which corresponds to the strongest near-resonance). We choose a/h_b=4, $b/h_b = 8$ and vary h_a/h_b; at each such h_a/h_b we use the iterative method described above to find the required zero of α_6. Table 1 shows the results of this procedure where the values of this zero are given alongside corresponding values of h_a/h_b. It is clear that the imaginary part is closer to zero the smaller h_a/h_b suggesting that resonance is stronger for shallower shoals. Indeed we can verify that smaller h_a/h_b corresponds to greater resonance in this case by solving the scattering problem with νh_b equal to the real part of the zero of α_6. The strength of the resonance is shown in the final column of table 1 where the maximum value of $|\phi_S/I|$, which measures wave amplification by the topography, is given.

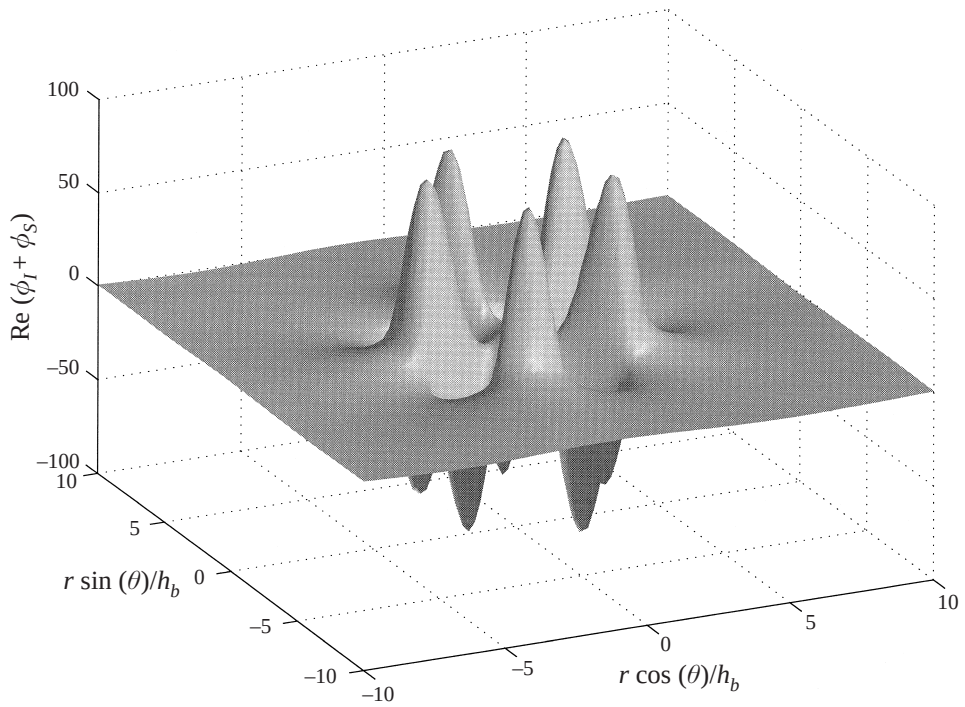

FIGURE 8. Surface plot of $\mathrm{Re}(\phi_I + \phi_S)$ for the example described in the text.

h_a/h_b	zero of α_6	$\max(\lvert\phi_S/I\rvert)$
0.05	$0.21764 - 7.9 \times 10^{-6}$i	237.92
0.06	$0.25274 - 3.0 \times 10^{-5}$i	117.85
0.07	$0.28580 - 9.2 \times 10^{-5}$i	66.125
0.08	$0.31690 - 2.4 \times 10^{-4}$i	40.452
0.09	$0.34611 - 5.3 \times 10^{-4}$i	26.842
0.10	$0.37348 - 1.1 \times 10^{-3}$i	18.902

TABLE 1. The zeros of α_6 for the example described in the text are given for a range of values of h_a/h_b. The strength of the resonance is indicated by the final column which shows an approximation to the factor by which the wave motion has been amplified. Five significant figures have been given for the real part of the zero and for $\max(\lvert\phi_S/I\rvert)$. Only two significant figures are given for the imaginary part of the zero since it is the size of this number which is of interest.

In figure 9 $|A_m|$ $(m = 0, 1, 2, \ldots, 15)$ are plotted against νh_b. The particular example we have considered is the submerged island of § 3.2, this time with $a/h_b = 5$, $b/h_b = 8$ and $h_a/h_b = 0.1$. The circles near the top of the graph show the real part of that zero of α_m with smallest positive real part. The dotted, vertical lines show that these zeros correspond closely to the first peak of $|A_m|$, as we have seen in other examples. Although figure 9 applies to a particular example, it exhibits certain features which we have also found in a wide range of numerical results for a variety of topographies. These features are as follows.

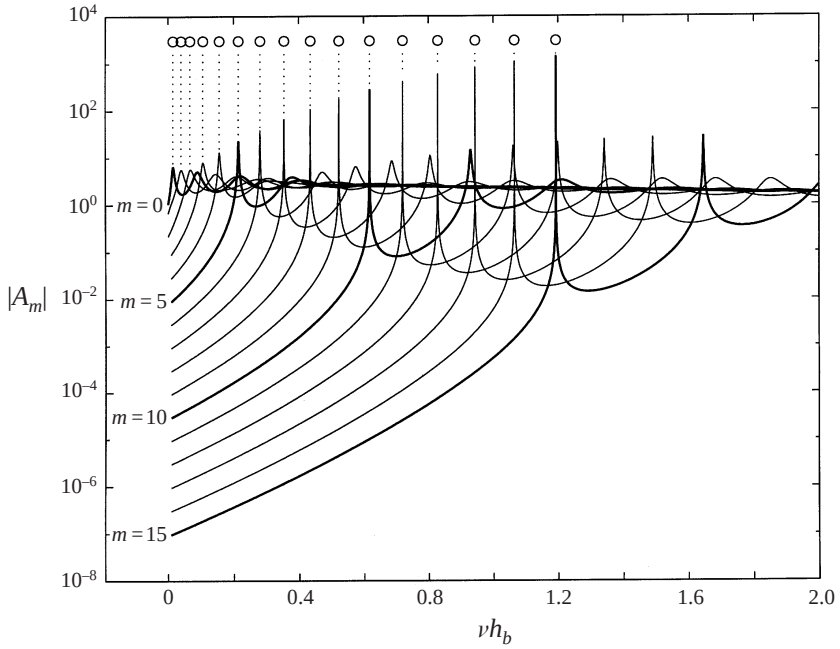

FIGURE 9. Graphs of $|A_m|$ (for $m = 0, 1, 2, \ldots, 15$) plotted against νh_b. The circles near the top of the figure show the position of the real part of a zero of $|A_m|$ (for $m = 0, 1, 2, \ldots, 15$). To aid clarity every fifth line has been plotted with a slightly thicker line.

(i) The pth local maximum of $|A_m|$ occurs at a larger value of νh_b than the pth local maximum of $|A_{m-1}|$, for $p, m = 1, 2, 3, \ldots$.

(ii) At all points to the left of the first peak of $|A_m|$, $|A_{m+p}| < |A_m|$ $p = 1, 2, 3, \ldots$.

(iii) The pth peak of $|A_m|$ is bigger than the $(p+1)$th peak $p, m = 1, 2, 3, \ldots$.

(iv) The height of the first peak of $|A_m|$ reaches a maximum value (with respect to m) and begins to decrease (this occurs in the current example for some $m > 15$).

(v) The larger the peak, the narrower its bandwidth. For example in the case considered in figure 9 $\max(|A_{15}|) > 1360$ was achieved at $\nu h_b = 1.193363$, but for $\nu h_b = 1.193293$ or 1.193423 then $|A_{15}| < 10$.

(vi) If νh_b is a value where $|A_m|$ has a local maximum, for some m, then for no other value of m does $|A_m|$ have a local maximum. This result can only be a conjecture at this stage; we believe that the result is true, but that peaks can become arbitrarily close. For example in figure 9 we can see that $|A_{15}|$ and $|A_{12}|$ have nearby peaks close to $\nu h_b = 1.2$.

One result of our observations is as follows and concerns when near-resonance is possible. We have noted in (i) above that the first peak of $|A_m|$ occurs at larger frequencies the larger m is. This means that, for a given value of νh_b, resonance is possible only in the first few modes. For example, from figure 9 we can see that, in this case, if $\nu h_b = 0.6$ then resonance is impossible in any mode higher than the ninth. This information can be used, together with (ii) above, to obtain an appropriate value for M in (3.1); if the first peak in $|A_m|$ occurs significantly to the right of the νh_b in hand then it is never necessary to consider modes higher than m.

5. Conclusions

We have used the modified mild-slope equation to approximate the diffraction of plane surface waves by axisymmetric bedforms, giving most attention to the effect of submerged circular shoals. As expected on the basis of previous work, near-resonance has been detected at a discrete set of frequencies for each topography which has been examined.

The solution for the free-surface profile can be expressed in terms of its Fourier modes and we have found that there is a distinct set of near-resonant frequencies for each mode. The smallest frequency in each set produces the largest free-surface response, each succeeding frequency giving rise to a weaker resonance than its predecessor. This effect has been explained by a reformulation of the problem which allows the solution to be examined in the phase plane. In this framework, near-resonance arises when part of the phase trajectory coincides with a branch of the stable manifold of a saddle-like structure. Successive near-resonant states correspond to additional half-circuits of the origin, before the stable manifold is encountered again.

One point worthy of note is that the frequencies which give rise to near-resonance generally fall outside the range of applicability of shallow water theory. An investigation of this problem using full linear theory would be formidable and our approach has the advantage of relative simplicity without the limitation of shallow water theory. As far as we are aware, there is no full linear solution available for axisymmetric scattering which will serve to examine the accuracy of the modified mild-slope equation for such geometry.

It should be noted that the modified mild-slope equation is a significant improvement on the mild-slope equation in many problems. This fact may be disguised in some of the examples we have considered. For example, Xu & Panchang's (1993) test problem discussed in § 3.1 is such that the dimensionless parameter kh is always sufficiently small that shallow water theory may reasonably be applied. In such a case both the mild-slope and modified mild-slope equations will predict solutions largely in agreement with shallow water theory (and therefore with each other). However we have encountered many examples in which the modified equation predicts scattered wave heights which differ from the mild-slope prediction by a factor of 2 or 3. This phenomenon occurs even when resonance is not present. Of course if we made such a comparison near the resonant frequencies discussed in this paper we could easily manufacture examples in which the differences between predictions made by the two approximations would be extremely large, but such cases are exceptional.

Qualitatively, our results are broadly in line with those previously obtained, which we have cited in § 1. For wholly submerged bedforms, the only model problem considered before consists of a circular cylinder and we have shown that the near-resonance phenomenon established in that case by Longuet-Higgins (1967) extends to arbitrary axisymmetric projections on an otherwise flat bed and that certain qualitative results carry over from the simpler topography. In particular, the smaller the relative water depth on the plateau, the greater the surface response above the projection at near-resonance. However, in the different problem of scattering around a conical island, Smith & Sprinks (1975) found that the near-resonant response increases with the mode number. In our examples for submerged topography, this is also the case up to a particular mode number, depending on the topography, beyond which the trend is reversed.

We have also examined the closely related phenomenon of near-trapping by considering the unforced problem with the previously imposed real frequency replaced by a

complex parameter. It transpires that trapping is not possible for any axisymmetric topography, but that near-trapping exists in the sense that there are real time-harmonic solutions of the homogeneous scattering problem with a superimposed exponentially small temporal decay.

REFERENCES

Berkhoff, J. C. W. 1973 Computation of combined refraction-diffraction. *Proc. 13th Intl Conf. on Coastal Engng, July 1972, Vancouver, Canada*, pp. 471–490 ASCE.

Berkhoff, J. C. W. 1976 Mathematical models for simple harmonic linear water waves. *Delft Hydr. Rep.* W 154-IV.

Black, J. L., Mei, C. C. & Bray M. C. G. 1971 Radiation and scattering of water waves by rigid bodies. *J. Fluid. Mech.* **46**, 151–164.

Booij, N. 1983 A note on the accuracy of the Mild-Slope equation. *Coastal Engng* **7**, 191–203.

Chamberlain, P. G. & Porter, D. 1995 The modified mild-slope equation. *J. Fluid Mech.* **291**, 393–407.

Hazard, C. & Lenoir, M. 1993 Determination of scattering frequencies for an elastic floating body. *SIAM J. Math. Anal.* **24**, 1458–1514.

Homma, S. 1950 On the behaviour of seismic sea waves around circular island. *Geophys. Mag. XXI*, 199–208.

Jordan, D. W. & Smith, P. 1977 *Nonlinear Ordinary differential equations.* Clarendon.

Lambert, J. D. 1992 *Numerical methods for Ordinary Differential Systems.* Wiley.

Lautenbacher, C. C. 1970 Gravity wave refraction by islands. *J. Fluid. Mech.* **41**, 655–672.

Longuet-Higgins, M. S. 1967 On the trapping of wave energy round islands. *J. Fluid. Mech.* **29**, 781–821.

Lozano, C. & Meyer, R. E. 1976 Leakage and response of waves trapped by round islands. *Phys. Fluids* **19**, 1075–1088.

Miles, J. M. 1986 Resonant amplification of gravity waves over a circular sill. *J. Fluid Mech.* **167**, 169–179.

Porter, D. & Staziker, D. J. 1995 Extensions of the mild-slope equation. *J. Fluid Mech.* **300**, 367–382.

Renardy, Y. 1983 Trapping of water waves above a round sill. *J. Fluid Mech.* **132**, 105–118.

Smith, R. & Sprinks, T. 1975 Scattering of surface waves by a conical island. *J. Fluid Mech.* **72**, 373–384.

Snodgrass, F. E., Munk, W. H. & Miller, G. R. 1962 Long-period waves over California's continental borderland. Part I: Background spectra. *J. Mar. Res.* **20**, 3–30.

Summerfield, W. 1972 Circular islands as resonators of long-wave energy. *Proc. R. Soc. Lond.* A **272**, 361–402.

Vastano, A. C. & Reid, R. O. 1967 Tsunami response for islands: verification of a numerical procedure. *J. Mar. Res.* **25**, 129–139.

Xu, B. & Panchang, V. 1993 Outgoing boundary conditions for finite-difference elliptic water-wave models. *Proc. R. Soc. Lond.* A **441**, 575–588.

Zhu, S. & Zhang, Y. 1996 Scattering of long waves round a circular island mounted on a conical shoal. *Wave Motion* **23**, 353–362.